Chromophore–Protein Interactions Affecting the Polyene Twist and π–π^* Energy Gap of the Retinal Chromophore in Schizorhodopsins

Taito Urui,[†] Tomomi Shionoya,[†] Misao Mizuno,[†#] Keiichi Inoue,[‡] Hideki Kandori,[§] and Yasuhisa Mizutani[†]*

[†] Department of Chemistry, Graduate School of Science, Osaka University, 1-1 Machikaneyama, Toyonaka, Osaka 560-0043, Japan

[‡] The Institute for Solid State Physics, The University of Tokyo, 5-1-5 Kashiwanoha, Kashiwa, Chiba 277-8581, Japan

[§] Department of Life Science and Applied Chemistry, Nagoya Institute of Technology, Showa-ku, Nagoya, Aichi 466-8555, Japan

ABSTRACT

The properties of a prosthetic group are broadened by interactions with its neighboring residues in proteins. The retinal chromophore in rhodopsins absorbs light, undergoes structural changes, and drives functionally important structural changes in the proteins during the photocycle. It is therefore crucial to understand how chromophore–protein interactions regulate the molecular structure and electronic state of chromophores in rhodopsins. Schizorhodopsin is a newly discovered subfamily of rhodopsins found in the genomes of Asgard archaea, which are extant prokaryotes closest to the last common ancestor of eukaryotes, and of other microbial species. Here, we report the effects of a hydrogen bond between a retinal Schiff base and its counterion on the twist of the polyene chain and the color of the retinal chromophore. Correlations between spectral features revealed an unexpected fact that the twist of the polyene chain is reduced as the hydrogen bond becomes stronger, suggesting that the twist is caused by tight atomic contacts between the chromophore and nearby residues. In addition, the strength of the hydrogen bond is the primary factor affecting color-tuning of the retinal chromophore in schizorhodopsins. The findings of the present study are valuable for manipulating the molecular structure and electronic state of the chromophore by controlling chromophore–protein interactions.

INTRODUCTION

The properties of prosthetic groups are regulated by interactions with their neighboring residues in proteins. A deeper understanding of this regulation can help engineer proteins with new functions. Rhodopsins are photoreceptive proteins containing retinal as a prosthetic group. The retinal chromophore is covalently linked to a Lys residue through a Schiff base. The chromophore is surrounded by seven transmembrane helices and interacts with nearby residues at several points. The protonated Schiff base is hydrogen-bonded to nearby residues and/or internal water molecules. The polyene chain of the retinal chromophore is situated between two specific aromatic residues, while an additional aromatic residue lies on the side of the polyene plane. These interactions play key roles in regulating the retinal chromophore in rhodopsins.[1] It is widely accepted that the selectivity of the photoisomerization site is determined by the steric effect due to residues surrounding the retinal chromophore in proteins because the photoproducts of all-*trans*-retinal derivatives in organic solvents are in the 7-*cis*, 9-*cis*, 11-*cis*, and 13-*cis* forms (numbering of the positions of the skeletal carbon atoms in the retinal chromophore is shown in Figure 1).[2] The electronic energy levels of the retinal chromophore are influenced by its interactions with charged, polar, and aromatic amino acids.[3] Quantum yields of the photoisomerization of the retinal chromophore are largely affected by the protonation state of the counterion of the Schiff base in a sodium ion-pumping rhodopsin, KR2,[4] and a proton-pumping rhodopsin, proteorhodopsin.[5]

Rhodopsins were previously categorized into two distinct types: type 1 and type 2.[6] Type 1 rhodopsins, known as microbial rhodopsins, were first isolated from *Halobacterium salinarum* and termed bacteriorhodopsin (*Hs*BR),[7] and later also isolated from diverse microorganisms spanning three domains of life (bacteria, archaea, and eukaryotes) and giant viruses. Type 2

rhodopsins, known as animal rhodopsins, are members of the G-protein-coupled receptor family. In 2018, functional metagenomics revealed a new family of rhodopsins, heliorhodopsin (HeR), which is distinct from both type 1 and type 2 rhodopsins.[8]

Schizorhodopsin (SzR) is a newly identified subfamily of rhodopsins found in the genome sequences of Asgard archaea, which are believed to be the closest extant prokaryotes to the last common ancestor of eukaryotes.[9] The first SzRs identified are light-driven inward proton pumps. Later, more SzRs were found from archaeal species living in high-temperature environments, such as SzRs from *Methanoculleus* sp. (*M*sSzR), and mesophilic *Methanoculleus taiwanensis* (*Mt*SzR)[10] and are also inward proton-pumping rhodopsins. A newly discovered inward proton-pumping rhodopsin identified in metagenomic sequences obtained from Antarctic freshwater lakes, referred to as Antarctic rhodopsin (AntR), shares a close phylogenetic relationship with SzR.[11] Although the specific role of inward proton transport by SzRs is not fully understood, it may play a crucial role in photosensory signaling or in maintaining cellular homeostasis.[11]

Phylogenetic analysis suggested that SzRs locate between type 1 rhodopsins and HeRs.[9] The amino acid sequences of SzRs exhibit similarities with those of both type 1 rhodopsins and HeRs. Figure 2 compares the amino acid resides around the retinal chromophore in *Hs*BR, SzR AM_5_00977 (SzR4), and HeR from *Thermoplasmatales* archaeon (*T*aHeR). In particular, Trp154 and Asp184 in SzR4 are analogous to Trp182 and Asp212 in *Hs*BR, respectively, while Trp68, Tyr71, and Phe157 in SzR4 are analogous to Trp106, Tyr109, and Phe206 in *T*aHeR, respectively. Therefore, the retinal binding pocket of SzRs is different from those of both type 1 rhodopsins and HeRs. These findings underscore the importance of exploring how interactions with neighboring residues influence the molecular structure and electronic state of the retinal chromophore in SzRs.

Herein, we report the molecular structure and electronic states of the retinal chromophore in the unphotolyzed SzRs, SzR AM_5S_00009 (SzR1), SzR SAMEA 2622822_312577 (SzR2), SzR TE_S2S_00499 (SzR3),[12] SzR4, *M*sSzR, and *Mt*SzR, and AntR, using UV–Vis absorption and resonance Raman spectroscopy. An extension of the spectroscopic study from our previous research[13] enabled us to investigate correlations between structural features and electronic states of the retinal chromophore in SzRs. The observed resonance Raman spectra showed a correlation between torsional distortions of the polyene chain and the strength of the hydrogen bond between the Schiff base and its counterion of the retinal chromophore, as well as that between the wavelength of the chromophore absorption and the hydrogen bond strength. Unexpectedly, polyene distortion decreased as the hydrogen bond became stronger in the SzRs, suggesting that the distortion is due to tight atomic contacts between the chromophore and the nearby residues. The positive correlation between the degree of distortion and the *cis–trans* thermal isomerization rate is consistent with our previous proposal that the tight contacts facilitate isomerization.[14] The present study revealed the effects of the tight contacts and the hydrogen bond of the Schiff base on the chromophore properties in SzRs, thereby shedding light on potential modifications to the properties of retinal proteins.

EXPERIMENTAL SECTION

Preparation of Protein Samples. *M*sSzR, *Mt*SzR, and AntR were expressed and purified by methods reported previously.[14] *Escherichia coli* (*E. coli*) C43(DE3) (Lucigen) containing a His-tagged SzR plasmid was cultivated in 2×YT at 37°C. Expression of SzRs in *E. coli* cells was induced by the addition of 1 mM isopropyl-β-D-thiogalactopyranoside and 10 μM all-*trans*-retinal (final concentration) when the optical density of the culture at 600 nm (OD_{600}) was over

6.0. Then, the cells were cultivated for 4 hours at 37°C and collected by centrifugation. The harvested *E. coli* cells containing each SzR were disrupted by ultrasonication. Following ultracentrifugation, the membrane fragments in the resulting supernatant were resuspended in 1.5% *n*-dodecyl-β-D-maltoside (DDM) in 20 mM MES–NaOH buffer (pH 6.5) containing 300 mM NaCl and 5 mM imidazole for AntR and in 1.5% DDM in 20 mM Tris–HCl buffer (pH 7.5) containing 150 mM NaCl and 10% glycerol for *M*sSzR and *Mt*SzR. The SzRs were solubilized in the buffers by stirring overnight at 4°C. *M*sSzR extracts were ultrasonicated prior to overnight solubilization to increase the degree of solubilization. Solubilized proteins were purified using a cobalt ion affinity column (Takara Bio, TALON Metal Affinity Resin). After loading on the column, proteins nonspecifically bound to the resin were removed by extensively washing the samples with 50 mM Tris–HCl buffer (pH 8.0) containing 300 mM NaCl, 15 mM imidazole, and 0.05% DDM for AntR and with 50 mM MES–NaOH buffer (pH 6.5) containing 300 mM NaCl, 5 mM imidazole, and 0.1% DDM for *M*sSzR and *Mt*SzR. The His-tagged SzRs were then eluted with 50 mM Tris–HCl buffer (pH 8.0) containing 300 mM NaCl, 1 M imidazole, and 0.05% DDM for AntR and with 50 mM MES–NaOH buffer (pH 6.0) containing 300 mM NaCl, 500 mM imidazole, and 0.1% DDM for *M*sSzR and *Mt*SzR.

Measurements of UV–Vis Absorption and Resonance Raman Spectra. UV–Vis absorption spectra of the protein samples were measured in the region of 250−700 nm using a spectrophotometer (Shimadzu, UV-3150). For resonance Raman measurements, the purified *M*sSzR and *Mt*SzR samples were suspended in 50 mM Tris–HCl buffer (pH 8.0) containing 100 mM NaCl, 300 mM Na_2SO_4, and 0.1% DDM. The purified AntR samples were suspended in Tris–HCl buffer (pH 9.0) containing 100 mM NaCl, 300 mM Na_2SO_4, and 0.1% DDM. The absorbance of the *M*sSzR, *Mt*SzR, and AntR sample solutions at maximum absorption

wavelength (λ_{max}) was set to 0.3 for a 2 mm path length. The UV–Vis absorption spectra of the samples used for the Raman measurements are shown in Figure S1. Detailed procedures for the resonance Raman measurements were described previously.[13] Briefly, the output of a single frequency CW diode-pumped laser with an operating wavelength of 532 nm (Cobolt, Samba 04-01) was used as the probe light. The probe laser power was set to 0.1 mW, which is sufficiently weak to avoid spectral contamination of long-lived photocycle intermediates. The 90° Raman scattering from samples placed in a Ø10 mm glass tube was collected and focused onto the entrance slit of a spectrograph (HORIBA Jobin Yvon, iHR320) equipped with a CCD camera (Roper Scientific, PyLoN:400B_eXelon VISAR). Both Rayleigh scattering and reflection of the probe light from the sample cell surface were eliminated by placing a short-cut dielectric filter (LV0550, Asahi Spectra) in front of the entrance slit. The Raman shifts were calibrated using the Raman bands of cyclohexane, acetone, and toluene.

RESULTS AND DISCUSSION

Resonance Raman Spectra of SzRs. The resonance Raman spectra of the unphotolyzed state of *M*sSzR, *Mt*SzR, and AntR in H_2O buffer are shown in Figure 3A. The overall features of the resonance Raman spectra of the three SzRs are similar and closely resemble those of SzR1, SzR2, SzR3, and SzR4, reported previously.[13] The present resonance Raman spectrum of AntR was comparable to the previous preresonance Raman spectrum of AntR in proteoliposomes at pH 8.[11] Based on normal-mode analysis of the retinal chromophore in *Hs*BR, the Raman bands in H_2O buffer observed at 1640–1643, 1528–1600, 1445–1474, 1349–1351, 1250–1322, 1162–1249, 1006–1007, and 813‑992 cm^{-1} were assigned to C=N stretching mode [ν(C=N)], C=C stretching mode [ν(C=C)], deformation mode of the methyl group, N–H rocking mode [δ(N–H)], C–CH

rocking mode [δ(C–CH)], C–C stretching mode [ν(C–C)], methyl rocking mode, and hydrogen-out-of-plane (HOOP) wagging mode, respectively.[15] Resonance Raman spectra of the unphotolyzed state of *M*sSzR, *Mt*SzR, and AntR in D_2O buffer are shown in Figure 3B. The ν(C=N) bands at 1640–1644 cm^{-1} in the H_2O buffer were shifted to 1618–1620 cm^{-1} in the D_2O buffer. The δ(N–H) bands at 1349–1351 cm^{-1} in the H_2O buffer were shifted to 967–969 cm^{-1} in the D_2O buffer. These deuteration shifts indicated that the Schiff base of the SzR chromophore was protonated.

The frequencies of the most intense ν(C=C) band differed between the three SzRs. The ν(C=C) frequency of AntR was lower than those of *M*sSzR and *Mt*SzR. This order is opposite to that of λ_{max} of the three SzRs (Figure S1). The ν(C=C) frequency exhibits an inverse correlation with λ_{max}.[16-17] Figure 4 shows plots of the frequency of the most intense ν(C=C) band against λ_{max} for the three SzRs in this study (red solid circles), the four SzRs reported previously[13] (red open circles), heliorhodopsins (blue open circles), and 19 typical microbial rhodopsins (gray open circles). The black line indicates the best-fit for a dataset of the 19 type 1 rhodopsins obtained using a linear function. The values of the three SzRs mostly fell within the frequency–wavelength distribution for type 1 rhodopsins previously reported. This correlation was attributed to the alternation in retinal π conjugation, in which the delocalization of π conjunction in the retinal polyene chain reduces the π–π^* energy gap and decreases the bond order of the C=C bonds.

Heliorhodopsins were previously reported to deviate from this frequency–wavelength distribution.[18] Interestingly, the values for six of the seven SzRs are on the lower frequency side of the fit. In particular, SzR1, SzR2, and SzR4 each showed similar but smaller deviations than those of heliorhodopsins. Another similarity between SzRs and heliorhodopsins was observed in

the shoulder band on the higher frequency side of the most intense ν(C=C) band. Heliorhodopsins exhibited a prominent shoulder band near the most intense ν(C=C) band,[18] whereas this prominent shoulder band was not observed in type 1 microbial rhodopsins and was thus attributed to the linear structure of the polyene chain.[19] For *Ms*SzR, *Mt*SzR, and AntR, a similar shoulder band was observed at 1548 cm^{-1}. Enlarged views of the ν(C=C) region of the spectra are shown in Figure S2. This feature was also observed for SzR1, SzR2, SzR3, and SzR4.[13] SzRs are present at a phylogenetically intermediate position between type 1 rhodopsins and heliorhodopsins.[12] The similarities of their spectral features suggest that the characteristics of the chromophore structure of SzRs are intermediate between those of type 1 rhodopsins and heliorhodopsins.

Figure 5 shows enlarged views of the HOOP band region from 925 to 1030 cm^{-1} for the three SzRs. Since the HOOP bands overlapped with each other and the methyl rocking band at 1006–1007 cm^{-1}, we decomposed the observed spectra into the component bands to determine the HOOP intensities. The frequencies and vibrational assignments of the HOOP bands are summarized in Table 1. The assignments are based on normal mode analysis for the all-*trans*-retinal chromophore in light-adapted *Hs*BR.[15] Linear polyenes exhibit normal modes of HOOP, which are linear combinations of the wagging modes.[20] The vibrational basis set comprises eight wagging modes associated with chain hydrogens. The presence of methyl groups on C_9 and C_{13} atoms subdivides the chain HOOP modes into three vibrationally isolated groups. Within these groups, the modes are expected to couple strongly across the double bonds and weakly across the single bonds.[15] Consequently, the $C_7H{=}C_8H$ and $C_{11}H{=}C_{12}H$ wagging modes are expected to be strongly coupled in the normal modes, whereas the $C_{10}H$ and $C_{14}H$ wagging modes likely remain relatively isolated. The $C_{15}H$ and NH wagging modes are less strongly coupled with each other

due to differences in the nature of carbon and nitrogen atoms. The HOOP vibrations can be categorized as in-phase (A_u symmetry) and out-of-phase (B_g symmetry) when they transform in the local symmetry point group (C_{2h}). The frequencies of in-phase modes are higher than those of out-of-phase modes.

The Raman intensities of HOOP modes increase when the polyene chain is torsionally distorted.[20] The most intense HOOP bands were observed at 993, 992, and 990 cm^{-1} for *Ms*SzR, *Mt*SzR, and AntR, respectively. They are assigned to the $C_{15}H$ wagging mode,[15] which is coupled with the NH wagging mode because the bands show deuteration shifts. Their high HOOP intensities show that the Schiff base segment of the polyene chain is twisted in the SzRs. The weak intensities of the other HOOP bands in the range 800–970 cm^{-1} indicate less twisting in the central segment of the polyene chain. A strong $C_{15}H$ HOOP and weak other HOOP bands were also observed in SzR1, SzR2, SzR3, and SzR4.[13] Accordingly, these spectral characteristics of the HOOP bands suggest that the torsional distortion of the polyene chain in the retinal chromophore is localized near the Schiff base and is common to all SzRs studied to date. Indeed, the crystallographic data for SzR4 show that the dihedral angles of C_{14}–C_{15}=N–C_ε are 146.0, 150.8, and 146.1° for three chains (PDB ID: 7E4G).[21]

A high $C_{15}H$ HOOP intensity of the retinal chromophore is uncommon for the unphotolyzed state of typical type 1 rhodopsins. However, the polyene chain of the chromophore can be distorted if the configuration is different from the all-*trans* form. In fact, the 13-*cis*-retinal chromophore in dark-adapted *Hs*BR exhibits a stronger HOOP band than the all-*trans*-retinal chromophore in light-adapted *Hs*BR.[15, 22] We examined the spectral features of the ν(C–C) bands of the chromophore because these features are sensitive to retinal configuration. Figure 6 shows the resonance Raman spectra in the ν(C–C) region for *Ms*SzR, *M*tSzR, and AntR in the H_2O and

D_2O buffers. Intense ν(C–C) bands were observed at 1162 and 1199 cm^{-1} for *Ms*SzR, 1162 and 1200 cm^{-1} for *Mt*SzR, and 1164 and 1199 cm^{-1} for AntR. This spectral feature of the ν(C–C) bands was also observed in light-adapted *Hs*BR containing an all-*trans*-retinal chromophore.[15] The ν(C–C) bands show a deuteration shift when the retinal configuration is in the 15-*syn* form.[23] No deuteration shift was observed for *Ms*SzR, *Mt*SzR, and AntR. Accordingly, the retinal chromophores in *Ms*SzR, *Mt*SzR, and AntR adopt the all-*trans* and 15-*anti* form and thus the retinal configurations of *Ms*SzR, *Mt*SzR, and AntR are similar to those of type 1 rhodopsins. This means that the distortion of the polyene chain arises not from the chromophore structure but from the retinal–protein interactions of SzRs.

Figure 7 shows enlarged views of the ν(C=N) bands for *Ms*SzR, *M*tSzR, and AntR in H_2O, D_2O, and H_2O/D_2O mixed buffers. The deuteration shift of the ν(C=N) band is well known to correlate with the strength of the hydrogen bond of the protonated Schiff base.[24] Fitting analysis showed that the deuteration shifts for the ν(C=N) bands of *Ms*SzR, *Mt*SzR, and AntR are 24.5, 25.9, and 22.6 cm^{-1} respectively, comparable to that in SzR1 (23 cm^{-1}), SzR2 (24 cm^{-1}), SzR3 (27 cm^{-1}), and SzR4 (23 cm^{-1}).[13] The deuteration shifts of the SzRs are larger than those of outward H^+ pumps (15–23 cm^{-1}),[15, 25-29] an outward Na^+ pump (22 cm^{-1}),[30] and inward Cl^- pumps (10–12 cm^{-1}).[31-32] Based on these results, SzRs mostly have a stronger hydrogen bond at the Schiff base than the other ion pumps studied to date.

The band width of the ν(C=N) band provides information on the hydrogen-bonding partner of the retinal Schiff base.[33] When the hydrogen-bonding partner is a water molecule, the band width of the ν(C=NH) band in H_2O buffer is wider than that of the ν(C=NH) band in mixed buffer due to vibrational energy transfer from the Schiff base to the water molecule. No band broadening

was observed in *M*sSzR, *Mt*SzR, and AntR; thus, the hydrogen-bonding partner is not a water molecule but an amino acid residue(s) in the protein.

Similarity of the Retinal Chromophore Structure in the SzR Family. The resonance Raman spectra of the unphotolyzed state revealed that the structural characteristics of the retinal chromophore in the seven SzRs (*M*sSzR, *Mt*SzR, AntR, SzR1, SzR2, SzR3, and SzR4) are similar to each other, particularly in terms of the strong hydrogen bond at the Schiff base and the torsional distortion of the retinal polyene chain near the Schiff base. The crystal structure of SzR4 shows that the Schiff base forms a hydrogen bond to Asp184.[21] The Asp residue near the Schiff base is well conserved in the SzR group (Figure S3). Thus, the Asp residue located one turn away from the Lys residue bound to the retinal chromophore in helix G is the likely partner of the strong hydrogen bond of the Schiff base.

Distortions of the Retinal Polyene Chain. We previously reported the high $C_{15}H$ HOOP intensity and large deuteration shift of the ν(C=N) mode for SzR1, SzR2, SzR3, and SzR4 and attributed these to the distortion of the polyene chain and strong hydrogen bond in the Schiff base as characteristics of SzRs.[13] In the present study, we similarly observed high $C_{15}H$ HOOP intensities and a large deuteration shift of the ν(C=N) mode for *M*sSzR, *Mt*SzR, and AntR. Figures 8A–D show plots of the area intensities of the $C_{15}H$ [$I(C_{15}H)$], $C_7H{=}C_8H$ [$I(C_7H{=}C_8H)$], $C_{11}H{=}C_{12}H$ [$I(C_{11}H{=}C_{12}H)$], and NH HOOP bands [I(NH)], respectively, relative to that of the methyl rocking band against the deuteration shift of the ν(C=N) band. We decomposed the spectral contributions of the HOOP bands for SzRs obtained in the previous study[13] and the results are shown in Figure S4. The intensity of the most intense HOOP band, $I(C_{15}H)$, exhibited a negative correlation with the ν(C=N) deuteration shift (correlation coefficient: r=−0.57). This negative correlation indicated that the distortion of the polyene chain near the Schiff base

becomes smaller as the hydrogen bond of the Schiff base to the counterion becomes stronger. This is contrary to what one would expect if the hydrogen bond was causing the distortion. Therefore, the negative correlation means that structural factors other than the hydrogen bond must be responsible for the distortion. Negative correlations with the deuteration shift were also observed for $I(C_7H{=}C_8H)$ (r=−0.68) and I(NH) (r=−0.44). In contrast, a positive correlation was observed for $I(C_{11}H{=}C_{12}H)$ and the ν(C=N) deuteration shift (r=0.79). The correlations would be either all positive or all negative if nothing other than the hydrogen bond causes the distortion. The nonuniform signs of the correlations suggest that both clockwise and counterclockwise twisted segments are present along the polyene chain direction. This nonuniformity is further strong evidence that the distortion of the polyene chain is caused not by the hydrogen bond between the Schiff base and the Asp residue but by other interactions with nearby residues. We recently proposed that tight atomic contacts between the $C_{13}{=}C_{14}$ group and nearby residues (Trp154 and Tyr71 in SzR4) facilitate the *cis–trans* thermal isomerization of SzRs.[14] Such tight contacts can distort the polyene chain near the Schiff base since protein structures are generally compact.[34]

The distortion of the retinal polyene chain can affect the barrier height for structural changes in the chromophore and thus their rate of change. We previously revealed that *cis–trans* reisomerization precedes reprotonation in the photocycle of SzRs.[14, 35] Therefore, we previously discussed the correlation between the rate of *cis–trans* reisomerization[14] and distortion of the retinal polyene chain. Figure 9 shows plots of the reisomerization rate against the HOOP intensities. The data for AntR, taken at pH 9, are plotted in the figure together with the data for the other six SzRs, taken at pH 8. We assume that the conversion rate from the early to late M intermediate is insensitive to pH because proton release and uptake likely occur during the

formation and decay of the M intermediate, respectively, and the decay rate of the M intermediate is insensitive to the bulk pH for SzR un_Tekir_02407.[36] Strong and positive correlations were observed between the reisomerization rate and the HOOP intensities in terminal regions of the polyene chain, I(NH) (r=0.59) and I(C_7H=C_8H) (r=0.71), implying that these distortions could facilitate reisomerization. The correlations between the reisomerization rate and the HOOP intensities, I($C_{11}H$=$C_{12}H$) and I($C_{15}H$), were weak, suggesting that these distortions do not facilitate reisomerization. Collectively, these results indicate that the reisomerization rate increases as the atomic contacts becomes tighter. This is consistent with our previous proposal that tight contacts distort the polyene chain and thus facilitate reisomerization by lowering its barrier height.[14]

Color Tuning of the Retinal Chromophore. Figure 10 shows plots of λ_{max} against the deuteration shift of the ν(C=N) mode and the HOOP intensities. Figure 10A shows a plot of λ_{max} against the deuteration shift of the ν(C=N) band and indicates a negative correlation between λ_{max} and the deuteration shift (r=−0.84). The negative charge in the counterion of the Schiff base stabilizes the positively charged nitrogen atom for the protonated retinal chromophore. Since the positive charge is more localized on the nitrogen atom in the electronically ground state than that in the electronically excited state, the hydrogen bond between the Schiff base and its counter ion increases the energy of the π–π^* electronic transition.[6] Accordingly, λ_{max} is shorter as the hydrogen bond becomes stronger, as observed in the present study. Thus, the observed negative correlation between λ_{max} and the hydrogen bond strength is well explained by the resonance structure of the π conjugation.

Figures 10B–D show plots of λ_{max} against I($C_{15}H$), I(C_7H=C_8H), I($C_{11}H$=$C_{12}H$), and I(NH), respectively. Positive correlations were observed except for against I($C_{11}H$=$C_{12}H$). The distortion

of the polyene chain strengthens the bond alternation of the π conjugation, resulting in a larger π–π^* energy gap. Therefore, the change in bond alternation explains the negative correlation. However, the HOOP intensities, except for the $C_{11}H{=}C_{12}H$ HOOP mode, show positive correlations with λ_{max}. These apparent positive correlations are due to an indirect effect of the hydrogen bond strength, which also reduces distortion of the polyene chain near the Schiff base. The present results indicate that the effect of the interaction of the counterion to the Schiff base on λ_{max} is stronger than that of the polyene distortion in SzRs. An attempt was previously made to determine the effect of the Asp184 counterion of the Schiff base in a D184N mutant of SzR4 on λ_{max}.[21] However, the D184N mutation rendered the protein colorless due to deprotonation of the Schiff base and thus the effect of the counterion of the Schiff base was not determined. The present study revealed that the strength of the hydrogen bond between the Schiff base and the counterion is the primary mode for color-tuning in SzRs.

CONCLUSIONS

In the present study, we revealed that the strong hydrogen bond of the Schiff base with the counterion reduces the degree of torsional distortion of the polyene chain near the Schiff base. This unexpected finding suggests that tight atomic contacts between the chromophore and nearby residues induce torsional distortion of the polyene chain. The observed positive correlations between NH HOOP intensity and the *cis–trans* reisomerization rate are consistent with the proposal that high atomic contacts facilitate *cis–trans* reisomerization prior to reprotonation at the Schiff base in the SzR photocycle. This strong hydrogen bond is the primary factor determining λ_{max} of the retinal chromophore in SzRs. The insights obtained in the present study

are helpful for controlling the molecular structure and electronic state of a chromophore in proteins in general by modification of chromophore–protein interactions.

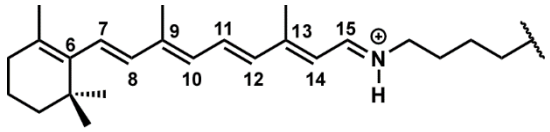

Figure 1. Numbering of the positions of the skeletal carbon atoms in the retinal chromophore.

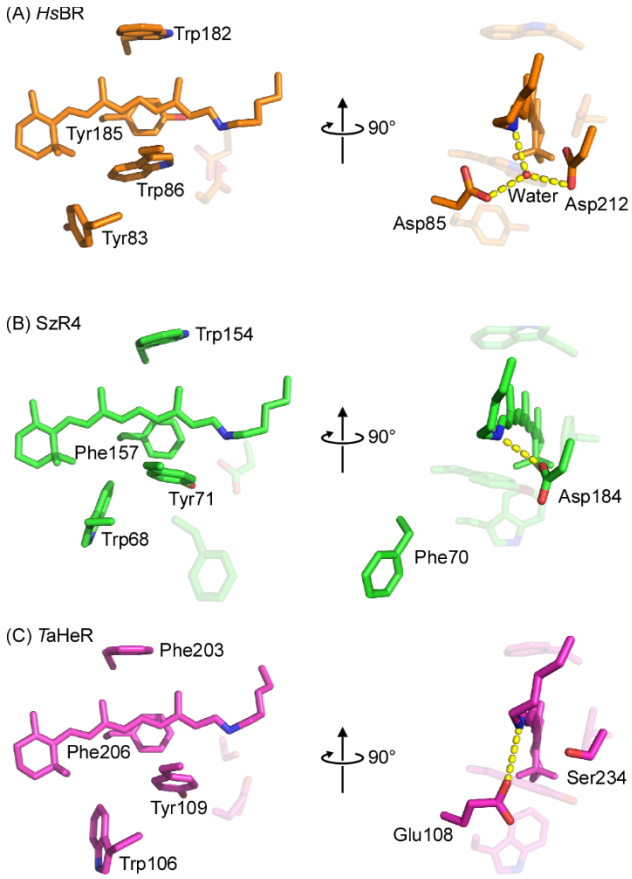

Figure 2. Comparison of amino acid resides around the retinal chromophore in *Hs*BR (A, PDB ID: 1C3W), SzR4 (B, PDB ID: 7E4G), and *T*aHeR (C, PDB ID: 6IS6). The red sphere in panel A represents the oxygen atom of the internal water molecule. Yellow dashed lines show hydrogen bonds.

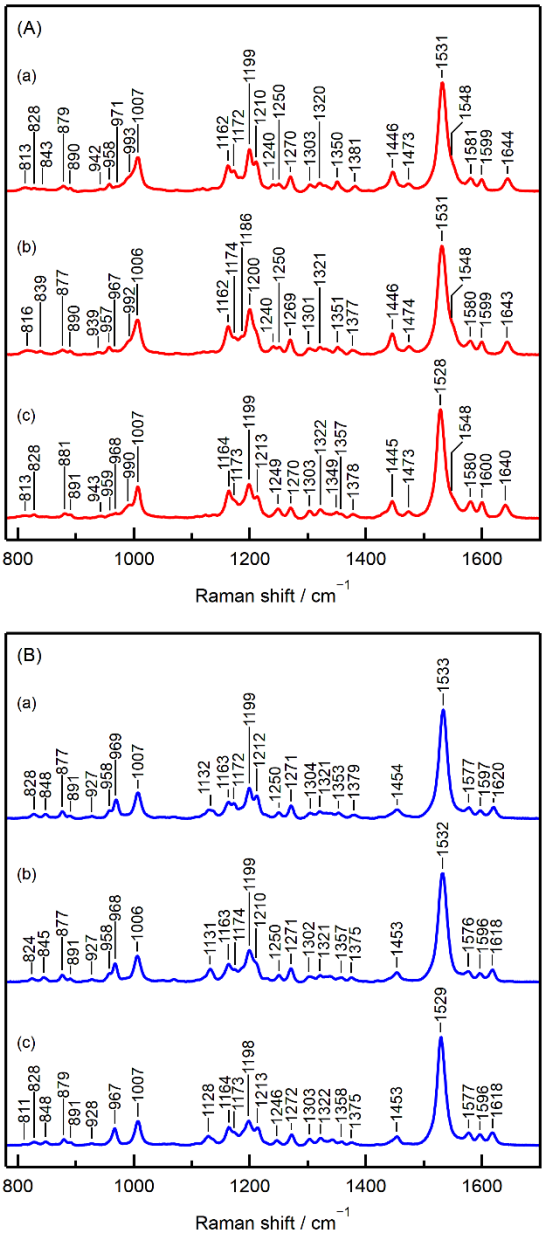

Figure 3. Resonance Raman spectra of the retinal chromophore of the unphotolyzed state in the SzRs in the H_2O (A) and D_2O buffers (B) obtained using a 532 nm probe light. In each panel, traces a, b, and c are for *Ms*SzR, *Mt*SzR, and AntR, respectively. The spectral contributions of the buffer and emission background have been subtracted.

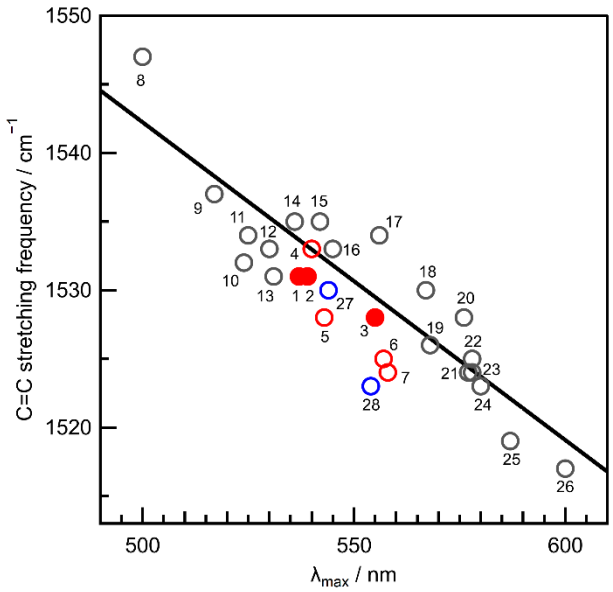

Figure 4. Plot of the frequency of the most intense C=C stretch mode against the maximum absorption wavelength for the retinal chromophore for the data sets of three SzRs in the present study (red open circles; 1: *Ms*SzR, 2: *Mt*SzR, 3: AntR), those of four SzRs (red solid circles; 4: SzR3, 5: SzR2, 6: SzR4, 7: SzR1), those of 19 microbial rhodopsins (gray circles; 8: *Natronomonas pharaonis* sensory rhodopsin II,[37] 9: K^+-bound *Krokinobacter* rhodopsin 2 (KR2),[38] 10: Na^+-bound KR2,[38] 11: *Indibacter alkaliphilus* sodium ion-pumping rhodopsin,[39] 12: thermophilic rhodopsin,[27] 13: cation-unbound KR2,[38] 14: Cl^--bound *Synechocystis* halorhodopsin (*Sy*HR),[40] 15: anion-depleted *Sy*HR,[40] 16: proteorhodopsin,[41] 17: SO_4^{2-}-bound *Sy*HR,[40] 18: NO_3^--bound *Halobacterium salinarum* halorhodopsin (*Hs*HR),[31] 19: *Hs*BR,[23] 20: Cl^--bound *Hs*HR,[31] 21, 22: Cl^--bound *Natronomonas pharaonis* halorhodopsin (*Np*HR),[32, 42] 23: Br^--bound *Np*HR,[32, 42] 24: I^--bound *Np*HR,[32] 25: *Halobacterium salinarum* sensory rhodopsin I,[43] 26: Anion-depleted *Np*HR[42]), and those of two heliorhodopsins (blue circles; 27: *Thermoplasmatales archaeon* SG8-52-1 heliorhodopsin,[18] 28: heliorhodopsin 48C12[18]). The frequency and the maximum absorption wavelength for *Ms*SzR, *Mt*SzR and AntR are the averages of two independent measurements.

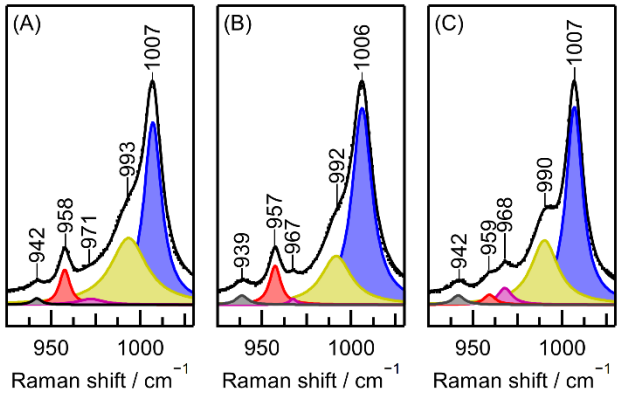

Figure 5. Enlarged views of the resonance Raman spectra in the HOOP mode region of *Ms*SzR (A), *Mt*SzR (B), and AntR (C) in H_2O buffer. The observed spectra are shown by black dots. Black curves indicate the best-fit for each spectrum using a linear combination of Lorentzian functions. Blue, yellow, purple, red, and gray areas indicate the integral intensities of the methyl rocking, $C_{15}H$, $C_7H{=}C_8H$, $C_{11}H{=}C_{12}H$, and NH HOOP bands obtained by curve fitting, respectively.

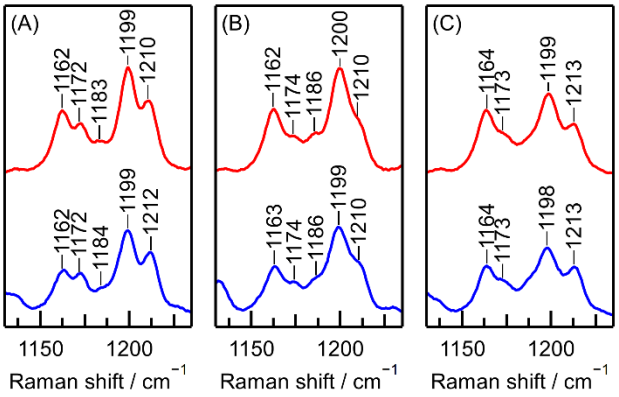

Figure 6. Enlarged views of the resonance Raman spectra in the ν(C-C) region of *M*sSzR (A), *Mt*SzR (B), and AntR (C). Red and blue traces indicate the resonance Raman spectra in the H_2O and D_2O buffers, respectively.

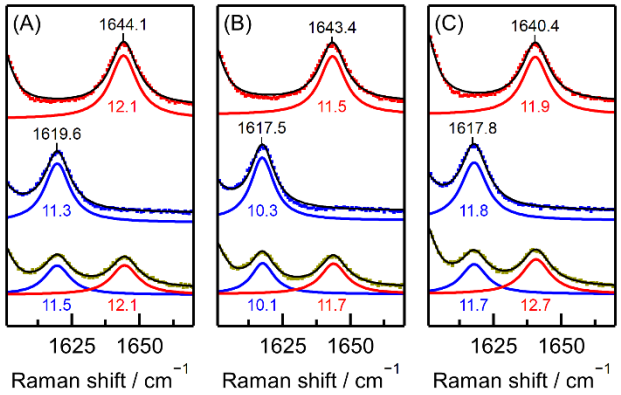

Figure 7. Enlarged views of the resonance Raman spectra in the ν(C=N) region of *M*sSzR (A), *Mt*SzR (B), and AntR (C). Red, blue, green dot curves indicate the resonance Raman spectra in the H_2O, D_2O, and mixed buffer (H_2O/D_2O = 1:1), respectively. Black curves indicate the best-fit for each spectrum using a linear combination of Lorentzian functions. Red and blue curves indicate the band shape of the ν(C=NH) and ν(C=ND) bands, respectively, obtained by curve fitting. The band widths are shown below each ν(C=N) band in the figure.

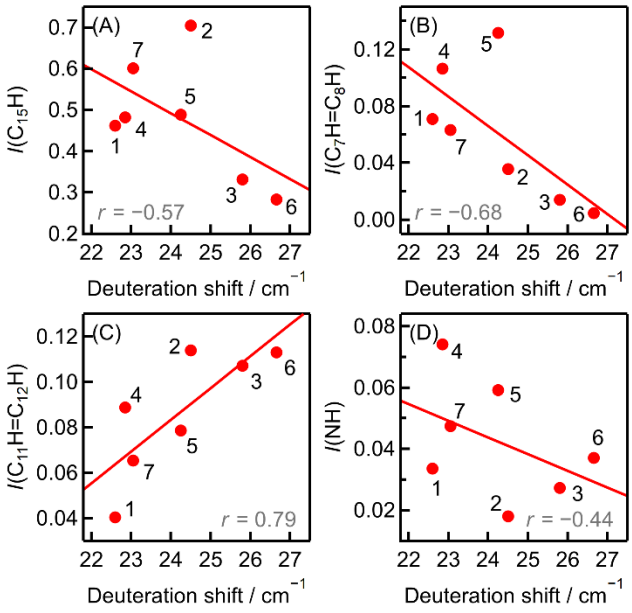

Figure 8. Plots of the area intensities of the $C_{15}H$ (A), $C_7H{=}C_8H$ (B), $C_{11}H{=}C_{12}H$ (C), and NH HOOP bands (D) relative to that of the methyl rocking band against the deuteration shift of the ν(C=N) band. The numbering for the markers is as follows. 1: AntR, 2: *Ms*SzR, 3: *Mt*SzR, 4: SzR1, 5: SzR2, 6: SzR3, 7: SzR4. The intensities and the deuteration shift for *Ms*SzR, *Mt*SzR and AntR are the averages from two independent measurements.

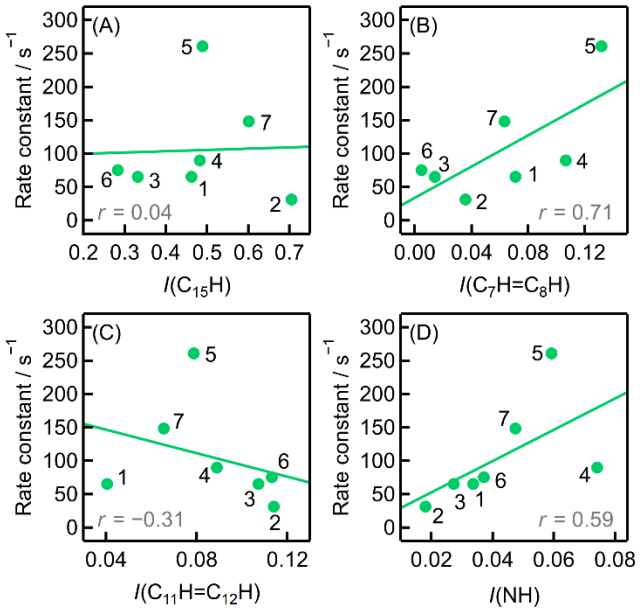

Figure 9. Plots of the rate constants of *cis-trans* reisomerization against the area intensities of the $C_{15}H$ (A), $C_7H{=}C_8H$ (B), $C_{11}H{=}C_{12}H$ (C), and NH HOOP bands (D) relative to that of the methyl rocking band. The numbering for the markers is the same as in Figure 8. The rate constants and intensities for *M*sSzR, *Mt*SzR and AntR are the averages from two independent measurements.

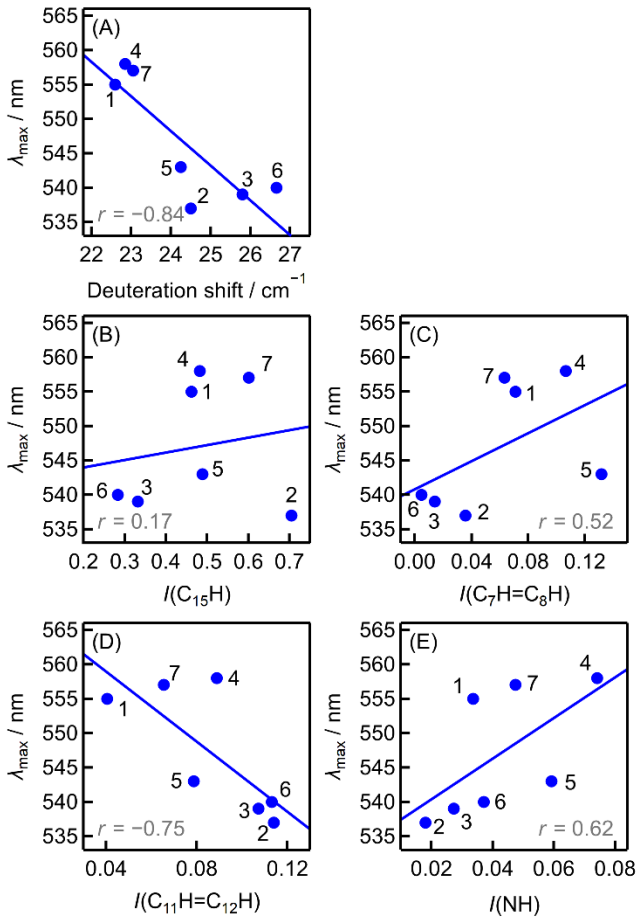

Figure 10. Plots of the absorption maximum wavelength against the deuteration shift of the ν(C=N) band (A) and the area intensities of the $C_{15}H$ (B), $C_7H{=}C_8H$ (C), $C_{11}H{=}C_{12}H$ (D), and NH HOOP bands (E) relative to the methyl rocking band. The numbering for the markers is the same as in Figure 8. The wavelength, deuteration shift, and intensity for *M*sSzR, *Mt*SzR and AntR are the averages from two independent measurements.

Table 1. Frequencies and assignments of the HOOP bands of *M*sSzR, *Mt*SzR, and AntR in H_2O buffer.

Frequency/cm^{-1}			Assignment
*M*sSzR	*Mt*SzR	AntR	
993	992	990	$C_{15}H$
971	967	968	$C_7H{=}C_8H$ A_u
958	957	959	$C_{11}H{=}C_{12}H$ A_u
942	939	942	NH

ASSOCIATED CONTENT

The Supporting Information is available free of charge on the ACS Publications website. UV–Vis absorption spectra of *M*sSzR, *Mt*SzR, and AntR, expanded views of the ν(C=C) region of the resonance Raman spectra of *M*sSzR, *Mt*SzR, and AntR in the H_2O buffer, amino acid residues around the retinal chromophore, and enlarged views of the resonance Raman spectra in the HOOP mode region for SzR1, SzR2, SzR3, and SzR4 in H_2O buffer are available in the Supporting Information. (PDF)

AUTHOR INFORMATION

Corresponding Author

Yasuhisa Mizutani — *Department of Chemistry, Graduate School of Science, Osaka University, 1-1 Machikaneyama, Toyonaka, Osaka 560-0043, Japan*; orcid.org/0000-0002-3754-5720; Email: mztn@chem.sci.osaka-u.ac.jp.

Present Addresses

[#] Department of Chemistry, Graduate School of Science, Kyoto University, Kitashirakawa-Oiwakecho, Sakyo-ku, Kyoto 606-8502, Japan; Email: misao@kuchem.kyoto-u.ac.jp.

Notes

The authors declare no competing financial interests.

ACKNOWLEDGMENT

This work was supported by a Grant-in-Aid for Japan Society for the Promotion of Science (JSPS) Fellows (JP22J22606, T.U.), and Grants-in-Aid for Scientific Research from the JSPS (JP20H02693, Y.M.; JP23H00285, Y.M.).

REFERENCES

1. Inoue, K., Photochemistry of the Retinal Chromophore in Microbial Rhodopsins. *J. Phys. Chem. B* **2023,** *127*, 9215-9222.
2. Freedman, K. A.; Becker, R. S., Comparative Investigation of the Photoisomerization of the Protonated and Unprotonated *N*-Butylamine Schiff Bases of 9-*cis*-, 11-*cis*-, 13-*cis*-, and All-*trans*-Retinals. *J. Am. Chem. Soc.* **1986,** *108*, 1245-1251.
3. Wang, W.; Nossoni, Z.; Berbasova, T.; Watson, C. T.; Yapici, I.; Lee, K. S. S.; Vasileiou, C.; Geiger, J. H.; Borhan, B., Tuning the Electronic Absorption of Protein-Embedded All-*trans*-Retinal. *Science* **2012,** *338*, 1340-1343.
4. Tahara, S.; Takeuchi, S.; Abe-Yoshizumi, R.; Inoue, K.; Ohtani, H.; Kandori, H.; Tahara, T., Origin of the Reactive and Nonreactive Excited States in the Primary Reaction of Rhodopsins: Ph Dependence of Femtosecond Absorption of Light-Driven Sodium Ion Pump Rhodopsin KR2. *J. Phys. Chem. B* **2018,** *122*, 4784-4792.
5. Chang, C.-F.; Kuramochi, H.; Singh, M.; Abe-Yoshizumi, R.; Tsukuda, T.; Kandori, H.; Tahara, T., Acid–Base Equilibrium of the Chromophore Counterion Results in Distinct Photoisomerization Reactivity in the Primary Event of Proteorhodopsin. *Phys. Chem. Chem. Phys.* **2019,** *21*, 25728-25734.
6. Ernst, O. P.; Lodowski, D. T.; Elstner, M.; Hegemann, P.; Brown, L. S.; Kandori, H., Microbial and Animal Rhodopsins: Structures, Functions, and Molecular Mechanisms. *Chem. Rev.* **2014,** *114*, 126-163.
7. Oesterhelt, D.; Stoeckenius, W., Rhodopsin-Like Protein from the Purple Membrane of *Halobacterium Halobium*. *Nature New Biol.* **1971,** *233*, 149-152.
8. Pushkarev, A.; Inoue, K.; Larom, S.; Flores-Uribe, J.; Singh, M.; Konno, M.; Tomida, S.; Ito, S.; Nakamura, R.; Tsunoda, S. P., et al., A Distinct Abundant Group of Microbial Rhodopsins Discovered Using Functional Metagenomics. *Nature* **2018,** *558*, 595–599.
9. Bulzu, P.-A.; Andrei, A.-Ş.; Salcher, M. M.; Mehrshad, M.; Inoue, K.; Kandori, H.; Beja, O.; Ghai, R.; Banciu, H. L., Casting Light on Asgardarchaeota Metabolism in a Sunlit Microoxic Niche. *Nature Microbiol.* **2019,** *4*, 1129-1137.
10. Kawasaki, Y.; Konno, M.; Inoue, K., Thermostable Light-Driven Inward Proton Pump Rhodopsins. *Chem. Phys. Lett.* **2021,** *779*, 138868.
11. Harris, A.; Lazaratos, M.; Siemers, M.; Watt, E.; Hoang, A.; Tomida, S.; Schubert, L.; Saita, M.; Heberle, J.; Furutani, Y., et al., Mechanism of Inward Proton Transport in an Antarctic Microbial Rhodopsin. *J. Phys. Chem. B* **2020,** *124*, 4851-4872.
12. Inoue, K.; Tsunoda, S. P.; Singh, M.; Tomida, S.; Hososhima, S.; Konno, M.; Nakamura, R.; Watanabe, H.; Bulzu, P.-A.; Banciu, H. L., et al., Schizorhodopsins: A Family of Rhodopsins from Asgard Archaea That Function as Light-Driven Inward H^+ Pumps. *Sci. Adv.* **2020,** *6*, eaaz2441.
13. Shionoya, T.; Singh, M.; Mizuno, M.; Kandori, H.; Mizutani, Y., Strongly Hydrogen-Bonded Schiff Base and Adjoining Polyene Twisting in the Retinal Chromophore of Schizorhodopsins. *Biochemistry* **2021,** *60*, 3050-3057.
14. Urui, T.; Hayashi, K.; Mizuno, M.; Inoue, K.; Kandori, H.; Mizutani, Y., *Cis–Trans* Reisomerization Preceding Reprotonation of the Retinal Chromophore Is Common to the Schizorhodopsin Family: A Simple and Rational Mechanism for Inward Proton Pumping. *J. Phys. Chem. B* **2024,** *128*, 744-754.

15. Smith, S. O.; Braiman, M. S.; Myers, A. B.; Pardoen, J. A.; Courtin, J. M. L.; Winkel, C.; Lugtenburg, J.; Mathies, R. A., Vibrational Analysis of the All-*trans*-Retinal Chromophore in Light-Adapted Bacteriorhodopsin. *J. Am. Chem. Soc.* **1987,** *109*, 3108-3125.
16. Aton, B.; Doukas, A. G.; Callender, R. H.; Becher, B.; Ebrey, T. G., Resonance Raman Studies of the Purple Membrane. *Biochemistry* **1977,** *16*, 2995-2999.
17. Kakitani, H.; Kakitani, T.; Rodman, H.; Honig, B.; Callender, R., Correlation of Vibrational Frequencies with Absorption Maxima in Polyenes, Rhodopsin, Bacteriorhodopsin, and Retinal Analogs. *J. Phys. Chem.* **1983,** *87*, 3620-3628.
18. Otomo, A.; Mizuno, M.; Singh, M.; Shihoya, W.; Inoue, K.; Nureki, O.; Béjà, O.; Kandori, H.; Mizutani, Y., Resonance Raman Investigation of the Chromophore Structure of Heliorhodopsins. *J. Phys. Chem. Lett.* **2018,** *9*, 6431-6436.
19. Urui, T.; Das, I.; Mizuno, M.; Sheves, M.; Mizutani, Y., Origin of a Double-Band Feature in the Ethylenic C═C Stretching Modes of the Retinal Chromophore in Heliorhodopsins. *J. Phys. Chem. B* **2022,** *126*, 8680-8688.
20. Eyring, G.; Curry, B.; Broek, A.; Lugtenburg, J.; Mathies, R., Assignment and Interpretation of Hydrogen out-of-Plane Vibrations in the Resonance Raman Spectra of Rhodopsin and Bathorhodopsin. *Biochemistry* **1982,** *21*, 384-393.
21. Higuchi, A.; Shihoya, W.; Konno, M.; Ikuta, T.; Kandori, H.; Inoue, K.; Nureki, O., Crystal Structure of Schizorhodopsin Reveals Mechanism of Inward Proton Pumping. *Proc. Natl. Acad. Sci. USA* **2021,** *118*, e2016328118.
22. Smith, S. O.; Pardoen, J. A.; Lugtenburg, J.; Mathies, R. A., Vibrational Analysis of the 13-*cis*-Retinal Chromophore in Dark-Adapted Bacteriorhodopsin. *J. Phys. Chem.* **1987,** *91*, 804-819.
23. Smith, S. O.; Lugtenburg, J.; Mathies, R. A., Determination of Retinal Chromophore Structure in Bacteriorhodopsin with Resonance Raman Spectroscopy. *J. Membr. Biol.* **1985,** *85*, 95-109.
24. Baasov, T.; Friedman, N.; Sheves, M., Factors Affecting the C=N Stretching in Protonated Retinal Schiff Base: A Model Study for Bacteriorhodopsin and Visual Pigments. *Biochemistry* **1987,** *26*, 3210-3217.
25. Miranda, M. R. M.; Choi, A. R.; Shi, L.; Bezerra, A. G.; Jung, K.-H.; Brown, L. S., The Photocycle and Proton Translocation Pathway in a Cyanobacterial Ion-Pumping Rhodopsin. *Biophys. J.* **2009,** *96*, 1471-1481.
26. Kralj, J. M.; Spudich, E. N.; Spudich, J. L.; Rothschild, K. J., Raman Spectroscopy Reveals Direct Chromophore Interactions in the Leu/Gln105 Spectral Tuning Switch of Proteorhodopsins. *J. Phys. Chem. B* **2008,** *112*, 11770-11776.
27. Shionoya, T.; Mizuno, M.; Tsukamoto, T.; Ikeda, K.; Seki, H.; Kojima, K.; Shibata, M.; Kawamura, I.; Sudo, Y.; Mizutani, Y., High Thermal Stability of Oligomeric Assemblies of Thermophilic Rhodopsin in a Lipid Environment. *J. Phys. Chem. B* **2018,** *122*, 6945-6953.
28. Saint Clair, E. C.; Ogren, J. I.; Mamaev, S.; Russano, D.; Kralj, J. M.; Rothschild, K. J., Near-IR Resonance Raman Spectroscopy of Archaerhodopsin 3: Effects of Transmembrane Potential. *J. Phys. Chem. B* **2012,** *116*, 14592-14601.
29. Waschuk, S. A.; Bezerra, A. G.; Shi, L.; Brown, L. S., *Leptosphaeria* Rhodopsin: Bacteriorhodopsin-Like Proton Pump from a Eukaryote. *Proc. Natl. Acad. Sci. USA* **2005,** *102*, 6879-6883.

30. Nishimura, N.; Mizuno, M.; Kandori, H.; Mizutani, Y., Distortion and a Strong Hydrogen Bond in the Retinal Chromophore Enable Sodium-Ion Transport by the Sodium-Ion Pump KR2. *J. Phys. Chem. B* **2019,** *123*, 3430-3440.
31. Maeda, A.; Ogurusu, T.; Yoshizawa, T.; Kitagawa, T., Resonance Raman Study on Binding of Chloride to the Chromophore of Halorhodopsin. *Biochemistry* **1985,** *24*, 2517-2521.
32. Mizuno, M.; Nakajima, A.; Kandori, H.; Mizutani, Y., Structural Evolution of a Retinal Chromophore in the Photocycle of Halorhodopsin from *Natronobacterium pharaonis*. *J. Phys. Chem. A* **2018,** *122*, 2411–2423.
33. Hildebrandt, P.; Stockburger, M., Role of Water in Bacteriorhodopsin's Chromophore: Resonance Raman Study. *Biochemistry* **1984,** *23*, 5539-5548.
34. Mizutani, Y., Time-Resolved Resonance Raman Spectroscopy and Application to Studies on Ultrafast Protein Dynamics. *Bull. Chem. Soc. Jpn.* **2017,** *90*, 1344-1371.
35. Hayashi, K.; Mizuno, M.; Kandori, H.; Mizutani, Y., *Cis–Trans* Reisomerization Precedes Reprotonation of the Retinal Chromophore in the Photocycle of Schizorhodopsin 4. *Angew. Chem. Int. Ed.* **2022,** *61*, e202203149.
36. Kojima, K.; Yoshizawa, S.; Hasegawa, M.; Nakama, M.; Kurihara, M.; Kikukawa, T.; Sudo, Y., Lokiarchaeota Archaeon Schizorhodopsin-2 (LaSzR2) Is an Inward Proton Pump Displaying a Characteristic Feature of Acid-Induced Spectral Blue-Shift. *Sci. Rep.* **2020,** *10*, 20857.
37. Gellini, C.; Lüttenberg, B.; Sydor, J.; Engelhard, M.; Hildebrandt, P., Resonance Raman Spectroscopy of Sensory Rhodopsin II from *Natronobacterium pharaonis*. *FEBS Lett.* **2000,** *472*, 263-266.
38. Otomo, A.; Mizuno, M.; Inoue, K.; Kandori, H.; Mizutani, Y., Allosteric Communication with the Retinal Chromophore Upon Ion Binding in a Light-Driven Sodium Ion-Pumping Rhodopsin. *Biochemistry* **2020,** *59*, 520-529.
39. Kajimoto, K.; Kikukawa, T.; Nakashima, H.; Yamaryo, H.; Saito, Y.; Fujisawa, T.; Demura, M.; Unno, M., Transient Resonance Raman Spectroscopy of a Light-Driven Sodium-Ion-Pump Rhodopsin from *Indibacter Alkaliphilus*. *J. Phys. Chem. B* **2017,** *121*, 4431-4437.
40. Niho, A.; Yoshizawa, S.; Tsukamoto, T.; Kurihara, M.; Tahara, S.; Nakajima, Y.; Mizuno, M.; Kuramochi, H.; Tahara, T.; Mizutani, Y., et al., Demonstration of a Light-Driven So_4^{2-} Transporter and Its Spectroscopic Characteristics. *J. Am. Chem. Soc.* **2017,** *139*, 4376-4389.
41. Krebs, R. A.; Dunmire, D.; Partha, R.; Braiman, M. S., Resonance Raman Characterization of Proteorhodopsin's Chromophore Environment. *J. Phys. Chem. B* **2003,** *107*, 7877-7883.
42. Gerscher, S.; Mylrajan, M.; Hildebrandt, P.; Baron, M.-H.; Müller, R.; Engelhard, M., Chromophore−Anion Interactions in Halorhodopsin from *Natronobacterium pharaonis* Probed by Time-Resolved Resonance Raman Spectroscopy. *Biochemistry* **1997,** *36*, 11012-11020.
43. Fodor, S. P.; Gebhard, R.; Lugtenburg, J.; Bogomolni, R. A.; Mathies, R. A., Structure of the Retinal Chromophore in Sensory Rhodopsin I from Resonance Raman Spectroscopy. *J. Biol. Chem.* **1989,** *264*, 18280-18283.

TOC graphic

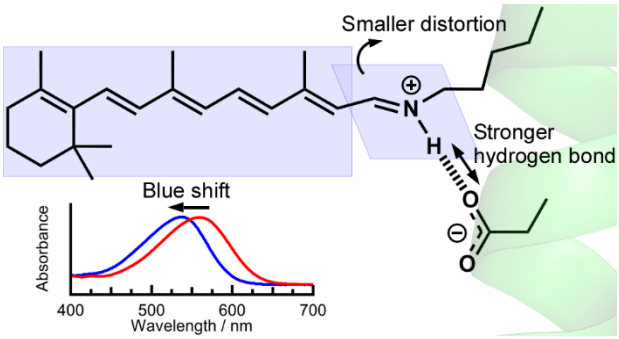
Smaller distortion
N
H
Stronger
hydrogen bond
O
O
Blue shift
Absorbance
400
500
600
700
Wavelength / nm